Appl Microbiol Biotechnol (1995) 44:27–36 

ORIGINAL PAPER

C. Zupke · A. J. Sinskey · G. Stephanopoulos

# Intracellular flux analysis applied to the effect of dissolved oxygen on hybridomas

Received: 20 September 1994/Received revision: 7 February 1995 / Accepted: 1 March 1995

**Abstract** Quantitative estimates of intracellular fluxes and measurements of intracellular concentrations were used to evaluate the effect of dissolved oxygen (DO) concentration on CRL 1606 hybridoma cells in batch culture. The estimates of intracellular fluxes were generated by combining material balances with measurements of extracellular metabolite rates of change. Experiments were performed at DO levels of 60% and 1% air saturation, as well as under oxygen-limited conditions. Cell extracts were analyzed to evaluate the effect of DO on the intracellular concentrations of the glutamate dehydrogenase reactants, as well as the redox state of the pyridine nucleotides in the cytosol and mitochondria. The relationship between cell density and pyridine nucleotide redox state was also investigated. Dissolved oxygen concentration had a significant effect on nitrogen metabolism and the flux through glutamate dehydrogenase was found to reverse at low DO, favoring glutamate formation. The NAD in the cytosol and mitochondria was more reduced under low DO conditions while the cytosolic NAD was more oxidized at low DO. Cytosolic NAD was reduced at higher cell densities while the redox states of cytosolic NADP and mitochondrial NAD did not exhibit significant variation with cell density. These results point to the fundamental role of the intracellular oxidation/reduction state in cell physiology and the possibility of controlling physiological processes through modulation of the dissolved oxygen level or the oxidation/reduction potential of the culture.

C. Zupke[1] · G. Stephanopoulos (✉)
Department of chemical Engineering, Biotechnology Process Engineering Center, Massachusetts Institute of Technology, Cambridge, MA 02139, USA

A. J. Sinskey
Department of Biology, Biotechnology Process Engineering Center, Massachusetts Institute of Technology, Cambridge, MA 02139, USA

*Present address:*

[1] Shriners Burns Institute, Cambridge, MA 02139, USA

## Introduction

Dissolved oxygen (DO) concentration is an important variable in the growth and metabolism of mammalian cells. Oxygen is essential for the efficient generation of ATP, and must be continually supplied to cultured cells because of its low solubility in water. In immobilized cell culture systems, as well as in tumors, oxygen gradients are likely to form at high cell densities, with some cells subjected to low DO conditions. In addition to its role as a substrate for the production of ATP, dissolved oxygen is also a major determinant of the medium redox potential. Medium redox potential is important because it correlates with cell density in fed-batch cultures of hybridomas and is influenced by growing cells (Hwang and Sinskey 1991).

Dissolved oxygen levels have been shown to have a variety of profound effects on cellular metabolism. For example, both growth rate and protein synthesis can be influenced by the level of dissolved oxygen (Boraston 1984; Mizrahi 1984; Reuveny et al. 1986; Miller et al. 1987; Phillips et al. 1987; Ozturk and Palsson 1990b), and nutrient consumption and waste production rates are also sensitive to DO. A frequently observed trend is that the specific glucose consumption and lactate production rates increase, and oxygen consumption rate decreases, once the DO drops below a critical value (typically between 1% and 10% of air saturation (Kilburn et al. 1969; Miller et al. 1987, 1988; Ozturk and Palsson 1990b; Siano and Mutharasan 1991). The metabolism of glutamine is also affected by the availability of oxygen. Both glutamine uptake and the yield of ammonia on glutamine have been found to change at low DO (Miller et al 1987; Ozturk and Palsson 1990b; Siano and Mutharasan 1991).

When studying the effects of oxygen on cellular metabolism, the pyridine nucleotides, NAD and NADP, become important because they participate in numerous reactions involving oxygen directly or indirectly. For example, transfer of electrons from NADH to oxygen is used to generate ATP, trans-plasma-membrane dehydrogenases can reduce oxygen (Crane et al. 1985), and NADPH provides reducing power to maintain levels of reduced glutathione, which serves to prevent the oxidation of protein thiols and is a principle scavenger of oxygen radicals (Kosower and Kosower 1978; Meister and Anderson 1983). The ubiquitous involvement of the pyridine nucleotides with dissolved oxygen provides many mechanisms by which oxygen can affect metabolism.

The quantification of intracellular fluxes under different DO levels, combined with measurements of intracellular concentrations or enzyme activities, can help to elucidate regulatory mechanisms in vivo. Intracellular fluxes can be estimated indirectly by combining a total mass or carbon balance with extensive measurements of the rates of change of extracellular metabolite concentrations. Carbon balances have been applied to flux estimation in a wide variety of biological systems including ecosystems (Klepper and Van de Kamer 1987), human respiration (Meersman and Faroudja 1988), microbial metabolism (Verhoff and Spradlin 1976; Reardon et al. 1987; Vallino and Stephanopoulos 1989), and rat heart metabolism (Safer and Williamson 1973). Since no isotopically labeled substrate is required, the estimation of fluxes from carbon or mass balances can be made in virtually any reactor system or scale.

In this work we used quantitative estimates of intracellular fluxes and measurements of intracellular concentrations to evaluate the effect of dissolved oxygen concentration on CRL 1606 hybridoma cells in batch culture.

## Materials and methods

### Cell line and medium

A murine hybridoma cell line, ATCC CRL 1606, producing an IgG against human fibronectin, was used in this study. To facilitate the measurement of carbon dioxide evolution, a Dulbecco's modified Eagle Medium (DMEM) formulation with HEPES buffer and reduced bicarbonate content was used. This formulation has a reduced requirement for $CO_2$ in the gas phase. The DMEM was prepared from powder and the final formulation contained 25 mM glucose, 4 mM glutamine, 10 mM HEPES, and 4 mM sodium bicarbonate. All media and chemicals were from Sigma. The medium was supplemented with 5% fetal bovine serum (Sigma, lot 47F0509).

### Bioreactor configuration and operation

Experiments were performed, in batch mode, in a 2-l CelliGen bioreactor model CL-25 (New Brunswick Scientific, Edison, N.J.), that had a cell-lift impeller. This reactor features automatic dissolved oxygen (DO), pH, and temperature controls. Surface aeration was used so the mesh screen surrounding the aeration cavity of the gas-exchange impeller was removed. The temperature was controlled at 36.8° C and agitation was set at 40 rpm. In the oxygen-limited run the feed oxygen was manually controlled so the specific oxygen transfer rate was significantly below normal aerobic values. Bottled air and nitrogen were used as the gas feed with their flow rates controlled by two flow meters (Aalborg Instruments, Monsey, N.Y.). The oxygen concentration in the feed stream was adjusted every 2 h to keep the specific oxygen-transfer rate approximately constant. In the 60% and 1% DO experiments the bioreactor controlled the DO by varying the flow of oxygen, nitrogen, and air into the reactor. In order to measure $CO_2$ evolution in the exit gas stream, $CO_2$ was not supplied for pH control. Nitrogen was connected to the $CO_2$ inlet instead and the pH controlled automatically at $7.27 \pm 0.02$ with the addition of base (6.1 g/l NaOH, 0.4 g/l KOH) pumped with a peristaltic pump (Cole Parmer, Chicago, Ill.). This base composition was chosen to be near the same osmolarity as the media, with the same Na/K ratio. An FC-260 mass-flow controller (Tylan Corp., Torrance, Calif.) was connected to the gas output from the CelliGen controller to ensure a constant gas flow rate of 100 ml/min. Samples were taken periodically and cell counts performed immediately with a hemocytometer and Coulter counter. The samples were centrifuged to remove cells and the supernatant frozen at $-70°$ C for subsequent analysis for extracellular metabolite concentrations.

### DO calibration

For the high-DO runs (DO = 60% of air saturation), the DO probe was calibrated to read 100 after equilibration with air. For the low-DO runs, a calibration curve was generated to relate the CelliGen bioreactor DO reading to the oxygen concentration as measured by an MGA-1200 mass spectrometer (Perkin-Elmer, Pomona, Calif.). The $O_2$ span was set to the maximum to provide the highest resolution at low DO and the true DO value obtained from the calibration curve. The calibration was checked upon completion of the experiment. In the low-DO experiments, the DO reading was found to have drifted by a value of less than 0.5% of air saturation.

### Oxygen-uptake rate

The oxygen-uptake rate (OUR) was measured by assuming that the oxygen in the liquid and gas phases were at pseudo-steady state:

$$\mathrm{OUR} = q_{O_2} N V = k_L a (c^* - c) V$$

where $q_{O_2}$ is the specific oxygen consumption rate, $N$ is the cell density, $V$ is reactor volume, $k_L a$ is the reactor mass-transfer coefficient, $c$ is the reactor oxygen concentration, and $c^*$ is the oxygen concentration in equilibrium with the gas phase. The oxygen-uptake rate was calculated from $k_L a$ (measured dynamically, without cells) combined with measured values for DO and $c^*$. $c^*$ was determined by analyzing the exit gas stream via a mass spectrometer. The solubility of oxygen in the culture medium at 37° C was calculated from empirical relationships to be $0.86\ \mathrm{mmol\,l^{-1}\,atm^{-1}}$ (Fleischaker 1982).

### $CO_2$ production rate

The $CO_2$ production rate (CPR) is the sum of the $CO_2$ evolution rate (CER) in the gas stream and the $CO_2$ (or bicarbonate ion) accumulation rate (CAR) in the medium:

$$\mathrm{CPR} = \mathrm{CER} + \mathrm{CAR}$$

$CO_2$ evolution was determined by monitoring the outlet gas $CO_2$ concentration and $CO_2$ accumulation was determined by differentiating a polynomial fit to the measured aqueous $CO_2$ content. Both these measurements have been described previously (Zupke and Stephanopoulos 1995).

### Rates of change of extracellular metabolites

The specific rates of change of glucose, lactate, and alanine were calculated by assuming constant specific productivity/consumption rates and exponential growth. The specific rates were found by a least-squares fit (using the Marquardt algorithm) of the concentration data to the following equation:

$$[S] = [S]_0 + \frac{q_s N_0}{\mu}(e^{\mu t} - 1)$$

where [S] is the measured concentration, $[S]_0$ is the initial concentration, $q_s$ is the specific uptake or consumption rate of S, $N_0$ is the initial cell number, and $\mu$ is the specific growth rate. Glutamine spontaneously decomposes to form ammonia and this must be taken into account when calculating the specific consumption rate of glutamine and the specific production rate of ammonia. The decomposition is first-order with a rate constant, $k_d$, of $0.017\ h^{-1}$ (measured in DMEM at the same temperature and pH as the reactor runs). Assuming constant specific productivity/consumption rates, exponential growth, and first-order decomposition of glutamine, the specific rates for glutamine and ammonia were found by fitting the concentration data to the following equations (Ozturk and Palsson 1990a):

$$[Gln] = [Gln]_0 e^{-k_d t} + \frac{q_{Gln} N_0}{k_d + \mu}(e^{\mu t} - e^{-k_d t})$$

$$[NH_3] = [NH_3]_0 + \left([Gln]_0 + \frac{q_{Gln} N_0}{k_d + \mu}\right)(1 - e^{-k_d t}) + \frac{N_0}{\mu}\left(q_{NH_3} - \frac{q_{Gln} k_d}{k_d + \mu}\right)(e^{\mu t} - 1)$$

### Cell extracts

Cell extracts were obtained by the technique of silicone oil layer centrifugation (Hwang 1992; Hwang et al. 1992). Centrifugation of the cells through a layer of silicone oil facilitates the rapid lysis of cells while excluding extracellular water. This allows for the accurate measurement of intracellular metabolites without the interference of the same compounds secreted in the medium. Approximately 200 ml cells was spun through a layer of silicone oil into a lysis buffer where the cells instantly lyse and all reactions stop. The lysis buffer consisted of 5% perchloric acid, 2% Triton X-100, and 41% $^2H_2O$ (Cambridge Isotope Labs, Cambridge, Mass.). The final density of the lysis solution was 1.05 g/ml. The silicone oil layer was made from AR 200 (1.049 g/ml, Fluka Chemie AG) and DC 200 (0.937 g/ml, Fluka Chemie AG) mixed in the ratio of 65 : 35 resulting in an oil layer density of 1.01 g/ml.

Custom-made glass tubes were used to perform the extraction. In the small-diameter bottom part 0.3–1.0 ml lysis solution was placed, followed by 1 ml silicone oil. Between 2 ml and 3 ml water was placed on top of the oil and the tubes were stored at $-20^\circ$C until needed. The top water layer permitted the rapid addition of medium with cells as it formed a barrier that prevented mixing of the oil layer. The tubes were spun at 1000 g for 15 min at 4 °C and the extract layer transferred to 1.5-ml eppendorf tubes and stored at $-70^\circ$C.

Before assays were performed on extracts, they were first neutralized by adding one-fifth the volume of 22.4% (w/v) $KHCO_3$/8.7% (w/v) KOH. This was performed on ice with repeated mixing to neutralize rapidly with as little loss of metabolites as possible. The $KClO_4$ precipitate was removed by centrifugation at $10^4$ *g* for 10 min at 4° C.

### Amino acid assays

Glutamine, glutamate, and alanine were analyzed with a Hewlet Packard 1090 Chem Station HPLC using a Hypersil C18 column (4 μm 10 cm × 2.1 mm inner diameter, Hewlet Packard) and diode array detector with a precolumn *o*-phthalaldehyde derivatization procedure. The mobile phase consisted of two solvents: (A) 7.1 g/l anhydrous $Na_2HPO_4$, 4.1 g/l anhydrous sodium acetate, 2% methanol, 2% tetrahydrofuran, pH = 7.5, and (B) 35% water in methanol (v/v). A flow rate of 0.35 ml/min was used with the following gradient: 90% A for 15.5 min, to 50% A after 16 min, to 44% A after 20 min, to 0% A after 20.5 min where it was held for 22.5 min. The derivatization was performed automatically using 4 μl 5 g/l *o*-phthalaldehyde solution and 8 μl sample. The sample was mixed with the *o*-phthalaldehyde for five cycles and the reaction allowed to proceed for 2 min before injection. The *o*-phthalaldehyde solution was prepared as follows: 50 mg *o*-phthalaldehyde was dissolved in 1 ml methanol plus 40 μl mercaptoethanol. This was diluted to 10 ml with borate buffer and 10 μl 30% aqueous Brij 35 surfactant was added. The borate buffer contained 12.36 g/l boric acid and 10.5 g/l KOH, and the pH was adjusted to 10.4 with KOH.

### Spectrophotometric metabolite assays

The analysis of samples from reactor runs for glucose, lactate, ammonia, and $CO_2$ was performed using assay kits (Sigma) 16-UV, 826-UV, 170-UV, and 132 respectively. Lactate in cell extracts was also analyzed with the spectrophotometer. With the exception of $CO_2$, all assays were performed on deproteinated samples. Reaction volumes were 1 ml and sample volumes were adjusted depending on expected concentrations present (usually between 7 μl and 100 μl).

### Fluorometric metabolite assays

Metabolites from cell extracts were measured fluorometrically by using NAD(P)-coupled enzymatic assays and enhancement of fluorescence with 6 M NaOH (Lowry and Passonneau 1972). For a few samples, isocitrate and oxaloacetate were assayed using larger volumes without fluorescence enhancement. The enzymes used in the metabolite assays were as follows: lactate dehydrogenase for pyruvate, malate dehydrogenase for malate and oxaloacetate, glutamate dehydrogenase for 2-oxoglutarate and ammonia, 3-hydroxybutyrate dehydrogenase for acetoacetate and 3-hydroxybutyrate, and isocitrate dehydrogenase for isocitrate. Fluorescence was measured with an LS-5 fluorimeter (Perkin Elmer). The excitation wavelength was 360 nm with a slit width of 10 nm and the emission wavelength was 460 nm with a slit width of 20 nm.

### Estimation of $NAD(P)^+$/NAD(P) H ratios

The redox state of the pyridine nucleotide pools were estimated using a well-established technique that takes advantage of near-equilibrium relationships (Krebs and Veech 1969; Bücher and Sies 1976; Tischler et al. 1977; Veech 1987). The oxidized and reduced metabolites, which are nearly in equilibrium with NAD or NADP, were measured and combined with the equilibrium constants to calculate the $NAD(P)^+$/NAD(P)H ratio. The enzymes believed to catalyze near-equilibrium reactions along with their equilibrium constants (at pH = 0 and cellular ionic strength) are (Veech 1987) lactate dehydrogenase, $1.11 \times 10^{-11}$ M; malate dehydrogenase, $2.86 \times 10^{-12}$ M; hydroxybutyrate dehydrogenase, $4.93 \times 10^{-9}$ M; glutamate dehydrogenase, $3.87 \times 10^{-13}$ $M^2$; isocitrate dehydrogenase

1.17 M; and malic enzyme, $3.44 \times 10^{-2}$ M. The enzymes are localized in either the cytosol or the mitochondria, so the calculated $NAD(P)^+/NAD(P)H$ ratios should represent the conditions in the compartment that contains the enzyme. Agreement between estimates of the $NAD(P)^+/NAD(P)H$ ratios obtained from independent reactions in the same compartment is strong evidence that the near-equilibrium assumption is valid. It is highly unlikely that two independent reaction systems would give similar values for the $NAD^+/NADH$ or $NADP^+/NADPH$ ratios unless both systems were near equilibrium and metabolites were relatively evenly distributed between the cytosol and mitochondria.

## Flux estimation from material balances

Intracellular fluxes were estimated using a method previously validated with $^{13}C$-NMR (Zupke and Stephanopoulos 1995).

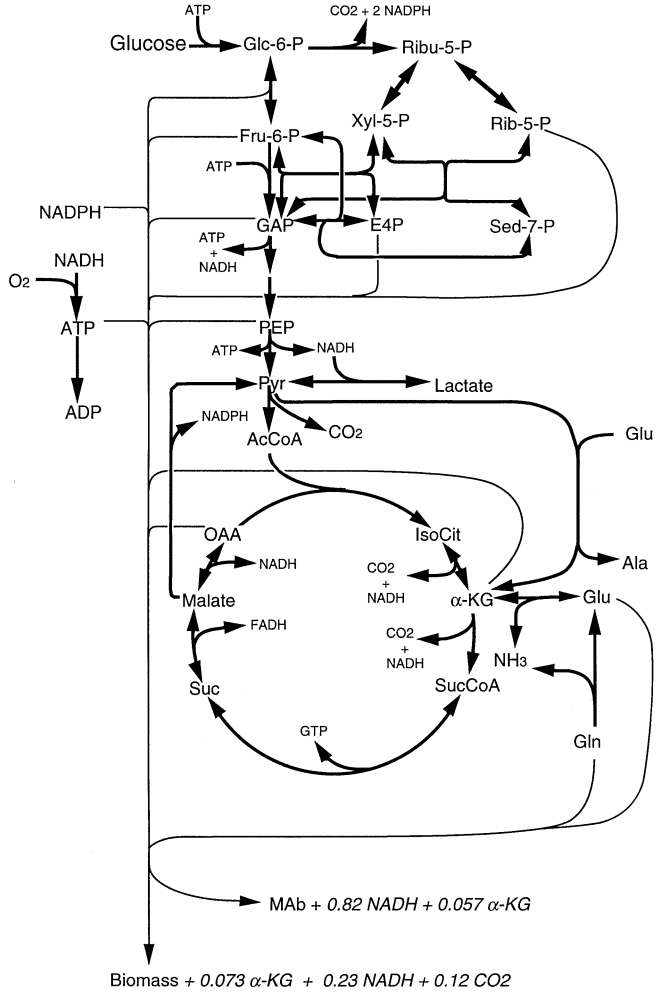


**Fig. 1** Biochemistry of energy metabolism, and biomass and antibody production. For clarity some glycolytic and tricarboxylic acid cycle intermediates, as well as $H_2O$, NAD, NADP, FAD, CoA, GDP, and ADP are not shown but are understood to be present when necessary. *Glc* glucose, *Fru* fructose, *Ribu* ribulose, *Rib* ribose, *Xyl* xylose, *E4P* erythrose-4-phosphate, *Sed* sedoheptulose, *GAP* glyceraldehyde-3-P, *PEP* phospho*enol*pyruvate, *Pyr* pyruvate, *AcCoA* acetyl-coenzyme A, *IsoCit* isocitrate, *α-KG* ketoglutarate (2-oxoglutarate), *SucCoA* succinyl-CoA, *Suc* succinate, *OAA* oxaloacetate, *Gln* glutamine, *Glu* glutamate, *Ala* alanine, *MAb* monoclonal antibody

**Table 1** The set of reactions describing energy metabolism in CRL-1606 hybridomas. This represents the network presented in Fig. 1 with some intermediates that are only involved in two reactions removed (*Glc* glucose, *Fru* fructose, *GAP* glyceraldehyde 3-phosphate, *Sed* sedoheptulose, *α-KG* α-ketoglutarate, i.e. 2-oxoglutarate)

| | |
|---|---|
| 1 | Glv + ATP → Glc-6-*P* + ADP |
| 2 | Glc-6-*P* → Fru-6-*P* |
| 3 | Fru-6-*P* + ATP → 2GAP + ADP |
| 4 | GAP + 2ADP + NAD → pyruvate + NADH + 2ATP |
| 5 | Pyruvate + NADH → lactate + NAD |
| 6 | Glc-6-*P* + 2NADP → ribulose-5-*P* + 2NADPH + $CO_2$ |
| 7 | Ribulose-5-*P* ↔ xylulose-5-*P* |
| 8 | Ribulose-5-*P* + xylulose-5-*P* ↔ Sed-7-*P* + GAP |
| 9 | Sed-7-*P* + GAP ↔ Fru-6-*P* + erythrose-4-*P* |
| 10 | Xylulose-5-P + erythrose-4-*P* ↔ Fru-6-*P* + GAP |
| 11 | Pyruvate + malate + 3NAD → α-KG + 3NADH + $2CO_2$ |
| 12 | α-KG + 2NAD + ADP → 2NADH + $CO_2$ + ATP + malate |
| 13 | Glutamine → glutamate + $NH_3$ |
| 14 | Pyruvate + glutamate → alanine + α-KG |
| 15 | Glutmate + NAD ↔ α-NADH + $NH_3$ |
| 16 | 2NADH + 6ADP + $O_2$ → 2NAD + 6ATP |
| 17 | Malate + NADP → pyruvate + $CO_2$ + NADPH |
| 18 | ATP → ADP |
| 19 | 0.036 glutamine + 0.062 glutamate + 0.0031 Glc-6-*P* + 0.013 Rib-5-*P* + 0.042GAP + 0.123 pyruvate + 0.019 malate + 0.74ATP + 0.188 NADPH + 0.23 NAD → biomass + 0.073 α-KG + 0.23 NADH + 0.12 $CO_2$ + 0.74 ADP + 0.188 NADP |
| 20 | 0.012 glutamine + 0.07 glutamate + 0.04 GAP + 0.011 NADPH + 0.012 malate + 0.082 NAD → Ab + 0.082 NADH + 0.057 α-KG + 0.011 NADP |

A matrix of stoichiometric coefficients (**A**) was constructed from the assumed biochemistry and used in formulating material balances for all key metabolites in the metabolic network. These balances can be represented in a compact form as $\mathbf{Ax} = \mathbf{r}$, where $\mathbf{x}$ is a vector of unknown intracellular fluxes and $\mathbf{r}$ is the vector of measured metabolite rates of change. The unknown fluxes were determined by the method of least squares. The uncertainties in measurements were incorporated by weighting the solution with the variance/covariance matrix, $\mathbf{P}$: $\mathbf{x} = (\mathbf{A}^T\mathbf{P}^{-1}\mathbf{A})^{-1}\mathbf{A}^T\mathbf{P}^{-1}r$. For strictly intracellular metabolites the pseudo-steady-state assumption was invoked and their rates of change taken to be zero. The biochemical network considered in this paper is shown in Fig. 1 and includes glycolysis, the pentose phosphate pathway, and tricarboxylic acid cycle. The reactions used to generate the matrix of stoichiometric coefficients are shown in Table 1. Those intermediates that are only involved in two reactions were eliminated to reduce the size of the problem (this is equivalent to setting their rates of change to zero). Lumped equations were used for biomass and antibody production (Zupke and Stephanopoulos 1995).

## Results

Three experimental conditions were investigated: normal DO (controlled at 60% of air saturation), low DO (controlled at 1% of air saturation), and oxygen-limited (with the oxygen-transfer rate controlled at $0.7 \times 10^{-10}$ mmol cell$^{-1}$ h$^{-1}$). The measured metabolic rates were reproducible with representative values shown in Figs. 2–5. The CRL 1606 hybridomas are insensitive to changes in DO between 5% and 60% (data not shown) but exhibit changes in metabolism at DO < 5%. The

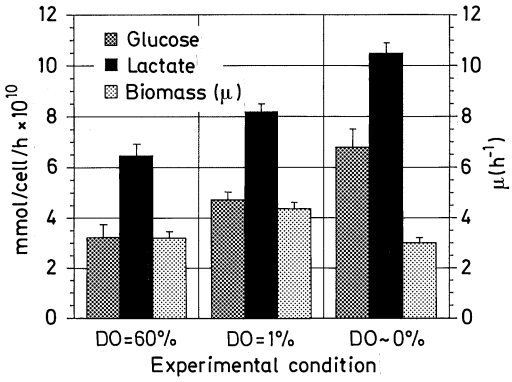


**Fig. 2** Specific rates of glucose consumption, and lactate and biomass production, at different dissolved oxygen (*DO*) concentrations

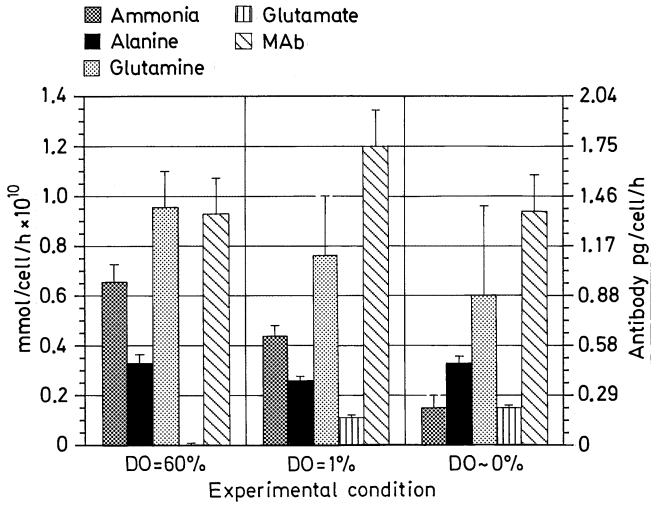


**Fig. 3** Specific rates of nitrogen-containing compounds at different dissolved oxygen (*DO*) concentrations. Glutamine is consumed while the other metabolites are produced. *MAb* monoclonal antibody

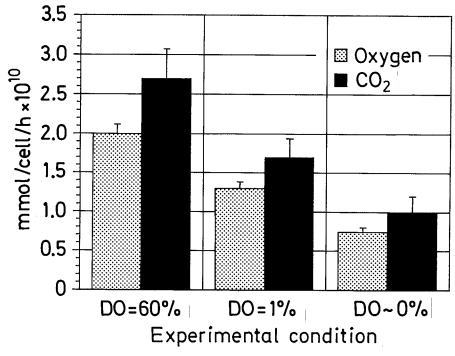


**Fig. 4** Specific oxygen consumption and $CO_2$ production rates at different dissolved oxygen (*DO*) concentrations

oxygen-uptake and $CO_2$ production rates decrease significantly while both glucose consumption and lactate production increase as the DO is reduced. The specific growth rate and specific antibody productivity exhibited

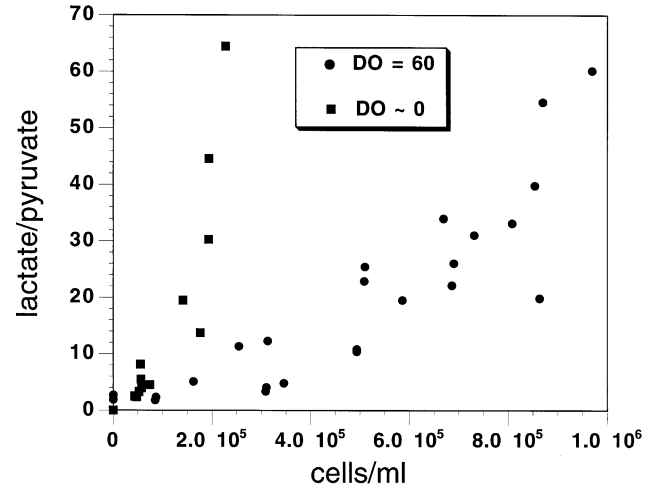


**Fig. 5** Lactate/pyruvate ratio as a function of cell density. The lactate/pyruvate ratio increases with cell density (or culture time). The high activity of lactate dehydrogenase keeps cytosolic $NAD^+$ and NADH in near equilibrium with lactate and pyruvate so these data indicate that cytosolic NAD becomes more reduced as cells grow. The $DO = 60\%$ data came from multiple reactor runs

a slight maximum at $DO = 1\%$. At lower DO there was a decrease in glutamine consumption and a dramatic decrease in ammonia production. While alanine production remained relatively constant, there was significant production of glutamate at low DO and essentially none at 60%. The significant reduction in the production of ammonia at low DO values, and the concomitant production of glutamate indicate an interesting response of the cellular metabolism to different oxygen levels.

To characterize further the effect of oxygen on cellular metabolism the intracellular fluxes were estimated from the measured rates of change. Table 2 summarizes the most important fluxes and their uncertainties. The flux of pyruvate into the tricarboxylic acid cycle is significant at normal DO but is only slightly positive at 1% and essentially zero under the oxygen-limited conditions. The flux through alanine aminotransferase is roughly constant at 30 f mol $cell^{-1}\,h^{-1}$. The flux through glutamate dehydrogenase is slightly positive at $DO = 60\%$ and significantly negative at low DO. A number of interesting quantities can be calculated from the fluxes through the biochemical network and are shown in Table 3. The total ATP produced dropped from 1.95 to 1.58 pmol $cell^{-1}\,h^{-1}$ when the DO was reduced. The fraction of ATP derived from glucose increased from 0.67 to 0.85 when the DO was reduced and parallels the fraction of ATP derived from glycolysis which increased from 0.34 to 0.69.

To examine the effect of oxygen on the glutamate dehydrogenase reaction and on pyridine-nucleotide redox states, intracellular concentrations of selected metabolites were measured. Glutamate, ammonia, and 2-oxoglutarate are easily measured in extracts and are

**Table 2** Selected flux estimate calculated from measured rates of change of extracellular metabolites (*TCA* tricarboxylic acid cycle, *GLDH* glutamate dehydrogenase, *DO* dissolved oxygen)

| Reaction | Flux (mol cell$^{-2}$ h$^{-1}$) DO = 0% | DO = 1% | DO = 60% |
|---|---|---|---|
| Pyruvate into TCA cycle | 0.0 ± 0.3 | 0.94 ± 0.3 | 0.28 ± 0.94 |
| Pyruvate to alanine | 0.33 ± 0.3 | 0.26 ± 0.2 | 0.33 ± 0.3 |
| Glu to 2-oxyglutarate via GLDH | −0.29 ± 0.3 | −0.14 ± 0.2 | 0.4 ± 0.3 |
| Malate to pyruvate | −0.24 ± 0.3 | 0.41 ± 0.3 | 0.59 ± 4 |

**Table 3** Quantitites derived from estimates of intracellular fluxes

| Quantity | DO ≈ 0% | DO = 1% | DO = 60% |
|---|---|---|---|
| Total ATP (pmol cell$^{-1}$ h$^{-1}$) | 1.58 | 1.67 | 19.5 |
| Fracton of ATP from glucolysis | 0.69 | 0.5 | 0.34 |
| Fraction of ATP from glucose | 0.85 | 0.75 | 0.67 |
| Fraction of lactate from gluose | 0.99 | 0.98 | 0.96 |
| Fraction of ATP for "maintanance" | 0.29 | 0.46 | 0.62 |

**Table 4** Intracellular metabolite concentrations from cell extracts. The means of three to six measurements ± standard error are shown

| Metabolite | Concentration (mM) | | | | |
|---|---|---|---|---|---|
| | DO = 60% $10^6$ cells/ml | DO = 60% $2.6 \times 10^5$ cells/ml | DO = 1% $9.2 \times 10^5$ cells/ml | DO = 1% $3.5 \times 10^5$ cells/ml | DO ~ 0% $2.6 \times 10^5$ cells/ml |
| 2-Oxoglutarate | 0.2 ± 0.03 | 0.32 ± 0.03 | 0.13 ± 0.01 | 0.17 ± 0.01 | 0.15 ± 0.006 |
| Isocitrate | 0.11 ± 0.02 | 0.038 ± 0.015 | 0.021 ± 0.002 | 0.034 ± 0.001 | 0.015 ± 0.0002 |
| Oxaloacetate | 0.05 ± 0.03 | 0.061 ± 0.015 | 0.0011 ± 0.001 | 0.0011 ± 0.001 | 0.002 ± 0.0006 |
| Glutamate | 1.8 ± 0.18 | 1.4 ± 0.2 | 4.2 ± 0.3 | 2.9 ± 0.2 | 2.5 ± 0.4 |
| Ammonia | 1.1 ± 0.1 | 0.8 ± 0.1 | 1.9 ± 0.1 | 1.2 ± 0.1 | 0.8 ± 0.1 |
| Lactate | 24 ± 10 | 3.2 ± 0.3 | 12 ± 2 | 12 ± 1 | 16 ± 3 |
| Pyruvate | 0.8 ± 0.1 | 0.36 ± 0.01 | 0.22 ± 0.02 | 0.3 ± 0.01 | 0.14 ± 0.01 |
| Malate | 5 ± 0.5 | 3.2 ± 0.4 | 0.67 ± 0.02 | 0.4 ± 0.02 | 0.48 ± 0.01 |
| $CO_2$ | 1.7 ± 0.1 | 2.6 ± 0.3 | 2.9 ± 0.1 | 2.3 ± 0.1 | 2.7 ± 0.1 |
| 3-Hydroxybutyrate | N.A. | 1.3 ± 0.1 | 2.4 ± 0.02 | 2.6 ± 0.02 | 2.6 ± 0.1 |
| Acetoacetate | N.A. | 1.7 ± 0.2 | 0.73 ± 0.1 | 1.06 ± 0.2 | 1.0 ± 0.2 |

instrumental in revealing the cause of the reversal of flux through glutamate dehydrogenase. Estimates of the free $NAD(P)^+/NAD(P)H$ ratios in the cytosol and the mitochondria were obtained using established near-equilibrium relationships and measured metabolite concentrations. Since mammalian cells tend to reduce their environment as they grow (Hwang and Sinskey 1991) it was expected that there may be a difference in $NAD(P)^+/NAD(P)H$ ratios at different cell densities. Analysis of extracellular pyruvate/lactate ratios indicated that there should be a continual reduction in the $NAD(P)^+/NAD(P)H$ ratio through the course of a culture (Zupke 1993) (see Fig. 5). To test for a possible correlation between cell density and the redox state of the different pools of pyridine nucleotides, extracts were obtained at two different cell densities at DO levels of 60% and 1%. Under the oxygen-limited conditions the cells would only grow to a low cell density so only one extract was obtained. The concentrations of the metabolites are shown in Table 4.

The resulting estimates of $NAD(P)^+/NAD(P)H$ ratios are presented in Table 5. Each ratio is estimated using two independent reaction systems (with the exception of the high-cell-density, DO = 60% experiment where mitochondrial $NAD^+/NADH$ was only estimated from glutamate dehydrogenase. There was good agreement between independent estimates, indicating that the assumption of near equilibrium and the uniform distribution of metabolites is most likely valid. The weighted averages of the $NAD(P)^+/NAD(P)H$ ratios are retabulated in Table 6. As anticipated from previous observations of extracellular lactate/pyruvate ratios, the cytosolic $NAD^+/NADH$ ratios decreased as cell density increased at a given DO level. However, cytosolic $NADP^+/NADPH$ and mitochondrial $NAD^+/NADH$ ratios did not vary significantly with cell density. Table 6 also shows that the cytosolic and mitochondrial $NAD^+/NADH$ ratios decreased at lower DO levels while the cytosolic $NADP^+/NADPH$ ratio increased at lower DO levels.

**Table 5** $NAD(P)^+/NAD(P)H$ ratios from metabolite concentrations ± estimated standard error. The two independent estimates for each quantity are combined to form the weighted average (*LDH* lactate dehyedrogenase, *MDH* malate dehydrogenase, *isoDH* isocitrate dehydrogenase, *ME* malic enzyme, *GLDH* glutamate dehydrogenase, *HBDH* hydroxybutyrate dehydrogenase)

| Experiment | Cytosolic NAD/NADH | | |
|---|---|---|---|
| | From DH | From ME | Average |
| DO = 60%, $10^6$ cells/ml | 300 ± 140 | 350 ± 210 | 315 ± 30 |
| DO = 60%, $2.6 \times 10^5$ cells/ml | 1000 ± 100 | 670 ± 180 | 920 ± 200 |
| DO = 1%, $9.2 \times 10^5$ cells/ml | 160 ± 30 | 55 ± 60 | 140 ± 60 |
| DO = 1%, $3.5 \times 10^5$ cells/ml | 220 ± 20 | 100 ± 70 | 210 ± 45 |
| DO ≈ 0%, $2.6 \times 10^5$ cells/ml | 76 ± 15 | 160 ± 40 | 90 ± 40 |
| | Cytosolic NADP/NADPH | | |
| | From isoDH | From ME | Average |
| DO = 60%, $10^6$ cells/ml | 0.0026 ± 0.0006 | 0.008 ± 0.001 | 0.004 ± 0.003 |
| DO = 60%, $2.6 \times 10^5$ cells/ml | 0.019 ± 0.008 | 0.009 ± 0.001 | 0.009 ± 0.002 |
| DO = 1%, $9.2 \times 10^5$ cells/ml | 0.016 ± 0.002 | 0.027 ± 0.002 | 0.022 ± 0.008 |
| DO = 1%, $3.5 \times 10^5$ cells/ml | 0.0099 ± 0.0008 | 0.05 ± 0.003 | 0.013 ± 0.014 |
| DO ≈ 0%, $2.6 \times 10^5$ cells/ml | 0.302 ± 0.003 | 0.02 ± 0.002 | 0.02 ± 0.002 |
| | Mitochondrial NAD/NADH | | |
| | From GLDH | From HBDH | Average |
| DO = 60%, $10^6$ cells/ml | 13 ± 3 | NA | 13 ± 3 |
| DO = 60%, $2.6 \times 10^5$ cells/ml | 19 ± 4 | 11 ± 2 | 13 ± 5 |
| DO = 1%, $9.2 \times 10^5$ cells/ml | 6.2 ± 0.8 | 2.5 ± 0.2 | 2.7 ± 1.2 |
| DO = 1%, $3.5 \times 10^5$ cells/ml | 7.4 ± 1 | 3.3 ± 0.2 | 3.5 ± 1 |
| DO ≈ 0%, $2.6 \times 10^5$ cells/ml | 5.0 ± 1 | 3.1 ± 0.4 | 3.1 ± 0.3 |

**Table 6** $NAD(P)^+/NAD(P)H$ ratios at different DO levels. Ratios are averages from Table 5. Low cell density = $2.6 \times 10^5$–$3.5 \times 10^5$ cells/ml and high cell density = $9 \times 10^5$ to $1 \times 10^6$ cells/ml

| | Ratio | | | |
|---|---|---|---|---|
| Cell density | Ratio estimated | Oxygen limited | DO = 1% | DO = 60% |
| Low | Cytosolic NAD/NADH | 90 ± 40 | 210 ± 45 | 920 ± 200 |
| | Cytosolic NADP/NADPH | 0.013 ± 0.014 | 0.02 ± 0.002 | 0.009 ± 0.002 |
| | Mitochondrial NAD/NADH | 3.1 ± 0.3 | 3.5 ± 1 | 13 ± 5 |
| High | Cytosolic NAD/NADH | | 140 ± 60 | 315 ± 30 |
| | Cytosolic NADP/NADPH | | 0.022 ± 0.008 | 0.004 ± 0.003 |
| | Mitochondrial NAD/NADH | | 2.7 ± 1.2 | 13 ± 3 |

## Discussion

It appears that a major effect of the reduction of DO is the reduction of the activity of the electron-transport chain, resulting in a decrease in mitochondrially produced ATP and a build-up of intracellular NADH. To compensate for the reduction in aerobic metabolism, the flux through glycolysis increases and results in an even greater production of lactate. However, this increase is not sufficient to maintain ATP production at the aerobic level. There is an estimated drop in ATP production of 14% and 19% in the 1% DO case and oxygen-limited case, respectively (Table 3). Interestingly, since the growth rates at low DO were slightly greater than, or comparable to that at normal DO (Fig. 2) the ATP fraction consumed for the production of biomass was thus slightly higher in the DO = 1% case and similar in the oxygen-limited case. This means that the ATP unaccounted for (consumed for "maintenance") exhibited a significant decline as the DO decreased. In the oxygen-limited case there is a 50% reduction in the fraction of ATP utilized for maintenance when compared to the DO = 60% case (Table 3).

This could be the result of the reduction in oxidative stress or a reduction in ATP wasted in futile cycles.

The flux estimates shown in Table 2 indicate some interesting features of glutamine metabolism and the tricarboxylic acid cycle. The primary pathway for the entrance of glutamine (through glutamate) into the cycle is via the transamination pathway, which results in the formation of alanine and 2-oxoglutarate. In addition, there is also 2-oxoglutarate associated with the production of biomass, which also occurs through transamination pathways. The direct deamination of glutamate via glutamate dehydrogenase is virtually inactive under normal DO conditions. At DO $\leq 1\%$ the transamination is essentially unchanged while a significant reverse flux occurs through glutamate dehydrogenase. This results in the accumulation of intracellular glutamate (Table 4) and its secretion into the medium (Fig. 3). The glutamate dehydrogenase reaction is driven backwards by the build-up of NADH as shown by the decreased $NAD^+/NADH$ ratio (Table 6). Although glutamate dehydrogenase can utilize both NAD and NADP as substrates, the agreement between the $NAD^+/NADH$ ratios obtained from glutamate and hydroxybutyrate dehydrogenases is strong evidence that the NAD pool is near equilibrium. Mitochondrial $NADP^+/NADPH$ ratios are typically comparable to cytosolic values (Zuurendonk et al. 1976), and 200-fold lower than mitochondrial $NAD^+/NADH$, owing to the activity of an energy-linked transhydrogenase. There is evidence that in rat liver mitochondria glutamate dehydrogenase is controlled at the NADPH-oxidizing reaction, which would prevent the equilibration of the NAD and NADP redox states (Wanders et al. 1983).

The dependence of cytosolic $NADP^+/NADPH$ on the DO level shows an opposite trend to that exhibited by the cytosolic and mitochondrial $NAD^+/NADH$ (Table 6). While the two NAD pools become more reduced at lower DO, the cytosolic NADP actually becomes more oxidized. This is somewhat surprising, given that all of the pyridine nucleotide pools are connected through shared reactants (Krebs and Veech 1969; Veech 1987). So a reduction in one system is likely to contribute to a reduction in another through the action of the near-equilibrium reactions that connect them. The observed results indicate that some process other than the near-equilibrium coupling is probably responsible. A likely candidate is the energy-linked transhydrogenase. In mammalian cells there is a mitochondrial membrane-bound enzyme that couples the transhydrogenation of NAD and NADP with the mitochondrial $H^+$ gradient. The characteristics of this enzyme, and possible physiological roles have been discussed elsewhere (Rydström et al. 1987; Hoek and Rydström 1988) and provide a possible explanation for the dependence of the $NADP^+/NADPH$ ratio on DO level. The transhydrogenase catalyzes the reaction:

$$NADH + NADP^+ \leftrightarrow NAD^+ + NADPH$$

and is coupled to the transfer of $H^+$ across the mitochondrial membrane. Hoek and Rydstrom (Rydström et al. 1987; Hoek and Rydström 1988) propose that the transhydrogenase could act as a buffer against changes in the mitochondrial proton gradient ($\Delta\mu_{H^+}$) or the $NAD(P)^+/NAD(P)H$ ratios. If the mitrochondria become de-energized so that $\Delta\mu_{H^+}$ is reduced, then the rate of the forward reaction is reduced and the rate of the reverse reaction is increased. This would result in a reduction in the NADPH produced and a higher $NADP^+/NADPH$ ratio. In the low-DO experiments there was a significant decrease in ATP produced aerobically, which may have been associated with a decrease in the $\Delta\mu_{H^+}$, and thus may explain the observed $NADP^+/NADPH$ ratios.

The cytosolic $NAD^+/NADH$ ratio was always inversely related to cell density. The reason why cytosolic NAD becomes more reduced at higher cell densities (or longer culture times) is not clear. It is known that cells reduce their medium in culture by secreting thiols (Hwang and Sinskey 1991) but the biological function, if any, of that reduction is not known. Given that the cellular environment becomes more reduced, an obvious question is whether the pyridine nucleotide redox is coupled to the electrical redox. The principle redox buffer within cells is glutathione (Kosower and Kosower 1978; Meister and Anderson 1983), which is maintained in a reduced state by the action of glutathione reductase:

$$GSSG + NADPH + H^+ \rightarrow 2GSH + NADP^+$$

However, intracellular redox (as shown by the GSH/GSSG ratio) is independent of cell density, even though the medium is continually reduced. Given that the extracellular environment becomes more reduced, another possible coupling mechanism to intracellular NAD(P)H redox is the activity of transplasma-membrane dehydrogenases. Numerous membrane-bound dehydrogenases have been found in mammalian cells, which can transfer electrons from NAD(P)H to extracellular substrates like oxygen, ferricyanide, and transferrin. The possible function of these dehydrogenases includes the transport of iron and amino acids, and the regulation of growth (Crane et al. 1985). A lowering of the redox potential of the medium should decrease the driving force for these transplasma-membrane dehydrogenases and would thus reduce the oxidation rate of intracellular NAD(P)H.

Another possible explanation of the continual reduction of the $NAD^+/NADH$ ratio involves the accumulation of lactic acid in the medium. Most cultured animal cells continuously secrete lactic acid as a result of high rates of aerobic glycolysis. Since both lactate and pyruvate pass freely through the plasma

membrane, their concentrations inside and outside the cell will be near equilibrium. Furthermore, because of the high activity of lactate dehydrogenase, the intracellular lactate and pyruvate will be in near equilibrium with cytosolic $NAD^+$ and NADH. Therefore, as lactate accumulates pyruvate will tend to accumulate as well. The production of pyruvate through glycolysis is coupled to the conversion of $NAD^+$ to NADH, and the conversion of pyruvate to lactate serves to regenerate $NAD^+$ from NADH. Thus, the accumulation of pyruvate will be associated with the net production of NADH. In addition, any consumption of pyruvate will result in the oxidation of lactate by $NAD^+$ to form pyruvate and NADH so that equilibrium is restored. Therefore, removal of pyruvate that is not associated with the regeneration of $NAD^+$ will serve to decrease the $NAD^+$/NADH ratio further. Pyruvate is consumed in several reactions including the tricarboxylic acid cycle and transamination with 2-oxoglutarate to form alanine. It is also known that pyruvate can act as an oxygen-radical scavenger (O'Donnel–Tormey et al. 1987) so that in the presence of oxygen there could be a continuous consumption of pyruvate, keeping its concentration artificially low. These features of pyruvate metabolism would then be reflected in the $NAD^+$/NADH ratio decreasing as lactate accumulated.

In summary, the analysis of intracellular fluxes using material balances and simple extracellular measurements has proved useful for the study of the effect of DO on hybridomas in batch culture. The results presented here demonstrate how estimates of the intracellular fluxes can be combined with measurements of intracellular metabolite concentrations to investigate the changes in energy metabolism that occur at low DO levels.

**Acknowledgements** The authors would like to acknowledge the support received from the Biotechnology Process Engineering Center at MIT and the National Science Foundation grant BCS-9311509.

## References

Boraston R, Thompson PW, Garland S, Birch JR (1984) Growth and oxygen requirements of antibody producing mouse hybridoma cells in suspension culture. Dev Biol Stand 55:103–111

Bücher T, Sies H (1976) Mitochondrial and cytosolic redox states in perfused rat liver:methods and problems in metabolic compartmentation. In:Tager JM, Söling HD, Williamson JR (eds). Use of isolated liver cells and kidney tubules in metabolic studies. North-Holland, Amsterdam, pp 41–64

Crane FL, Sun IL, Clark MG, Grebing C, Löw H (1985) Transplasma-membrane redox systems in growth and development. Biochim Biophys Acta 811:233–264

Fleischaker RJ (1982) An experimental study in the use of instrumentation to analyze metabolism and product formation in cell culture. PhD thesis, Massachusetts Institute of Technology

Hoek JB, Rydström J (1988) Physiological roles of nicotinamide nucleotide transhydrogenase. Biochem J 254:1–10

Hwang C (1992) The analysis of intracellular and extracellular redox states in cell culture. PhD thesis, Biochemical Engineering, Massachusetts Institute of Technology

Hwang C, Sinskey AJ (1991) The role of oxidation reduction potential in monitoring growth of cultured mammalian cells. In:Spier RE, Griffiths JB, Meigner B (eds) Production of biologicals from animal cells in culture. Halley Court, Oxford, pp 548–567

Hwang C, Sinskey AJ, Lodish HF (1992) Oxidized redox state of glutathione in the endoplasmic reticulum. Science 257:1496–1502

Kilburn DG, Lilly MD, Self DA, Webb FC (1969) The effect of dissolved oxygen partial pressure on the growth and carbohydrate metabolism of mouse LS cells. J Cell Sci 4:25–37

Klepper O, Van de Kamer JPG (1987) The use of mass balances to test and improve the estimates of carbon fluxes in an ecosystem. Math Biosci 85:37–49

Kosower NS, Kosower EM (1978) The glutathione status of cells. Int Rev Cytol 54:109–160

Krebs HA, Veech RL (1969) Pyridine nucleotide interrelations. In: Papa S, Tager JM, Quagliariello E, Slater EC (eds). The energy level and metabolic control in mitochondria. Adriatica, Bari, pp 329–382

Lowry OH, Passonneau JV (1972) A flexible system of enzymatic analysis. Academic Press, New York

Meersman RED, Faroudja NY (1988) Computerized substrate utilization determinations from respiratory functions alone. Comput Biol Med 18:449–453

Meister A, Anderson ME (1983) Glutathione. Annu Rev Biochem 52:711–760

Miller WM, Wilke CR, Blanch HW (1987) Effects of dissolved oxygen concentration on hybridoma growth and metabolism in continuous culture. J Cell Physiol 132:524–530

Miller WM, Wilke CR, Blanch HW (1988) Transient responses of hybridoma metabolism to changes in the oxygen supply rate in continuous culture. Bioprocess Eng 3:113

Mizrahi A (1984) Oxygen in human lymphoblastoid cell line cultures and effect of polymers in agitated and aerated cultures. Dev Biol Stand 55:93–102

O'Donnel–Tormey J, Nathan CF, Lanks K, DeBoer CJ, Harpe J de la (1987) Secretion of pyruvate:an antioxidant defense of mammalian cells. J Exp Med 165:500–514

Ozturk SS, Palsson BØ (1990a) Chemical decomposition of glutamine in cell culture media:effect of media type, pH, and serum concentration. Biotechnol Prog 6:121–128

Ozturk SS, Palsson BØ (1990b) Effects of dissolved oxygen on hybridoma cell growth, metabolism, and antibody production kinetics in continuous culture. Biotechnol Prog 6:437–446

Phillips HA, Scharer JM, Bols NC, Moo–Young M (1987) Effect of oxygen on antibody productivity in hybridoma culture. Biotechnol Lett 9:745–750

Reardon KF, Scheper T-H, Bailery JE (1987) Metabolic pathway rates and culture fluorescence in batch fermentations of *Clostridium acetobutylicum*. Biotechnol Prog 3:153–167

Reuveny S, Velez D, Macmillan JD, Miller L (1986) Factors affecting cell growth and monoclonal antibody production in stirred reactors. J Immunol Methods 86:53–59

Rydström J, Persson B, Carlenor E (1987) Transhydrogenases linked to pyridine nucleotides. In:Dolphin D, Avromovic O, Poulson R (eds) Pyridine nucleotide coenzymes. Wiley, New York, pp 433–460

Safer B, Williamson JR (1973) Mitochondrial-cytosolic interactions in perfused rat heart. J Biol Chem 248:2570–2579

Siano SA, Mutharasan R (1991) NADH fluorescence and oxygen uptake responses of hybridoma cultures to substrate pulse and step changes. Biotechnol Bioeng 37:141–159

Tischler ME, Friedrichs D, Coll K, Williamson JR (1977) Pyridine nucleotide distributions and enzyme mass action ratios in hepatocytes from fed and starved rats. Arch Biochem Biophys 183:222–236

Vallino JJ, Stephanopoulos G (1989) Flux determination in cellular bioreaction networks:applications to lysine fermentations. In: Sikdar SK, Bier M, Todd P (eds) Frontiers in bioprocessing. CRC, Boca Raton, Fla, pp 205–219

Veech RL (1987) Pyridine nucleotides and control of metabolic processes. In: Dolphin D, Avromovic O, Poulson R (eds) Pyridine nucleotide coenzymes. Wiley, New York, pp 79–104

Verhoff FH, Spradlin JE (1976) Mass and energy balance analysis of metabolic pathways applied to citric acid production by *Asperigillus niger*. Biotechnol Bioeng 18:425–432

Wanders RJA, Meijer AJ, Groen AK, Tager JM (1983) Bicarbonate and the pathway of gluatamate oxidation in isolated rat-liver mitochondria. Eur J Biochem 133:245–254

Zupke C (1993) Metabolic flux analysis in mammalian cell culture. PhD thesis, Chemical Engineering, Massachusetts Institute of Technology

Zupke C, Stephanopoulos G (1995) Intracellular flux analysis in hybridomas using mass balances and in vitro $^{13}C$ NMR. Biotechnol Bioeng 45:292–303

Zuurendonk PF, Akerboom TPM, Tager JM (1976) Metabolite distribution in isolated rat-liver cells and equilibrium relationships of mitochondrial and cytosolic dehydrogenases. In: Tager JM, Söling HD, Williamson JR (eds). Use of isolated liver cellls and kidney tubules in metabolic studies. North-Holland, Amsterdam, pp 17–27